SOFiSTiK


Benchmark Example No. 60

# Takeda Implicit Hinge with Cyclic Loading

SOFiSTiK | 2026

**VERiFiCATiON**
**BE60 Takeda Implicit Hinge with Cyclic Loading**

VERiFiCATiON Manual, Service Pack 2026-2 Build 16



**SOFiSTiK AG**

HQ Nuremberg
Flataustraße 14
90411 Nürnberg
Germany

T +49 (0)911 39901-0
F +49(0)911 397904

Office Garching
Parkring 2
85748 Garching bei München
Germany

T +49 (0)89 315878-0
F +49 (0)89 315878-23

info@sofistik.com
www.sofistik.com



**Front Cover**

| Overview | |
|---|---|
| **Element Type(s):** | B3D |
| **Analysis Type(s):** | DYN |
| **Procedure(s):** | MNL, TSTP |
| **Topic(s):** | |
| **Module(s):** | FEABENCH |
| **Input file(s):** | takeda_hinge.dat |

# 1 Problem Description

The structure is a very stiff, almost massless cantilever that is subjected to a cyclic lateral force applied at the top (cf. Fig. 1). The nonlinear behavior of the system is modeled using a concentrated plasticity approach —a plastic hinge— positioned at the base of the cantilever. The backbone curve of the plastic hinge follows an elasto-plastic model with hardening, and its hysteretic behavior under cyclic loading and unloading is captured using the modified Takeda model [1, 2] (cf. Fig. 2).

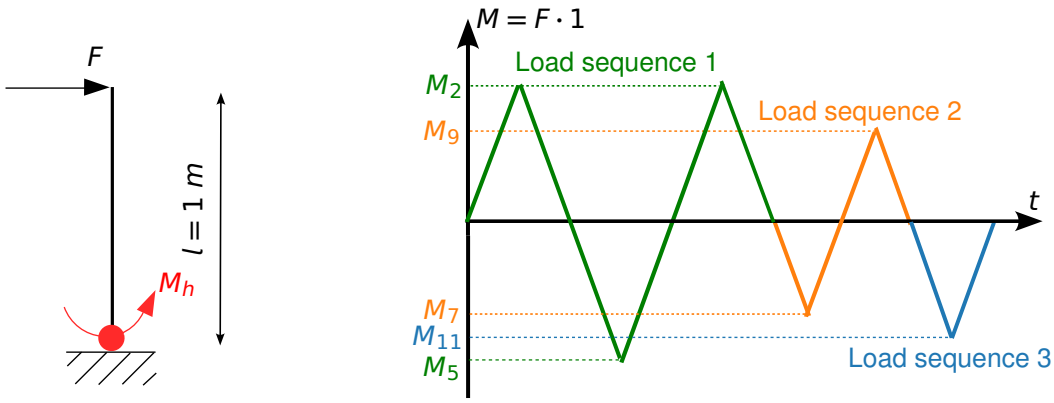


Figure 1: Problem description and load protocol. The loading is symetrical: $M_2 = |M_5|$, $M_9 = |M_7|$

The example verifies the behavior of the modified Takeda model in capturing the hysteretic response. This model is commonly used to describe the behavior of reinforced concrete components under seismic loading. Its formulation consists of a set of rules that define hysteretic moment-rotation cycles (or ”loops”) based on the previous loading-unloading history. The algorithmic rules are given as follows (see the *FEABENCH* manual for further information):

1. Monotonic extension: The response force is obtained directly from the backbone curve for a deformation which has not previously occurred.

2. Unloading: The tangent stiffness is obtained as

$$k_u = k_l \left( \frac{\phi_y}{\phi_m} \right)^{\alpha}, \tag{1}$$

   where $k_l$ is the elastic stiffness, $\phi_y$ is the yield deformation, $\phi_m$ is the maximum deformation experienced throughout the loading history, and $\alpha$ is an empirical exponent that adjusts the unloading slope.

3. Reloading: If the path remains within the largest internal loop, the response follows a straight line to that loop’s apex (cf. Fig. 2 (b)). Otherwise, it intersects the backbone curve at the deformation

$\phi_m$ on the targeted side, optionally shifted by

$$\beta\phi_d = \beta(\phi_m - \phi_y)\,, \tag{2}$$

where $\beta$ provides an additional calibration of the reloading path (cf. Fig. 2 (a)).

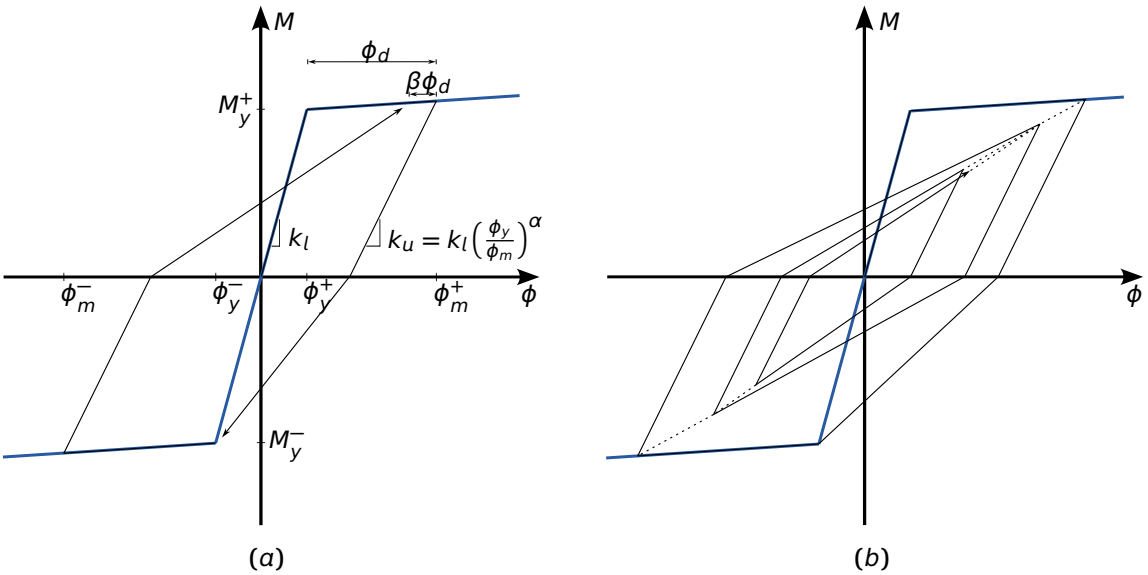


Figure 2: Modified Takeda model: ($a$) loading and large amplitude load reversal; ($b$) small amplitude load reversal

By selecting the cantilever's length to be 1 m, the excitation force $F$ and the moment in the plastic hinge $M$ become equal in magnitude. The base rotation is almost entierly dictated by the implicit hinge as the stiffness is very high relative to the beam bending stiffness (i.e. there is no beam bending). Moreover, since the structure is almost massless and the cyclic loading is applied relatively slowly, a quasi-static response can be observed, despite performing a dynamic analysis.

## 2 Theoretical Response of the Modified Takeda Model

In this section, we define analytical rules that determine the rotation of the plastic hinge under the loading shown in Fig. 1 (right), which consists of three loading sequences, including loading and unloading in both the positive and negative directions.

First, we define the yield moment $M_y$ and ultimate moment $M_u$, along with their corresponding rotations $\phi_y$ and $\phi_u$, to describe the backbone of the worklaw (cf. Fig. 3). We assume that the backbone is isotropic, i.e., the hinge exhibits identical behavior under positive and negative loading. With this backbone and the algorithmic rules defined in the previous section, we can analytically compute the rotation of the plastic hinge under the quasi-static loading.

We then define the following moment magnitudes relative to the yield moment $M_y$ and ultimate moment $M_u$ of the worklaw's backbone, with the goal of observing nonlinear behaviour:

$$M_y < M_2 = M_5 < M_u\,, \qquad 0 < |M_7| = M_9 < M_2\,, \qquad |M_7| < |M_{11}| < M_u\,. \tag{3}$$

This defines the cyclic loading, and using Takeda's hysteretic rules, we can obtain the corresponding cyclic moment-rotation curves, as depicted in Fig. 3.

Before explaining the moment-rotation behaviour in detail, we define the following stiffness parameters:

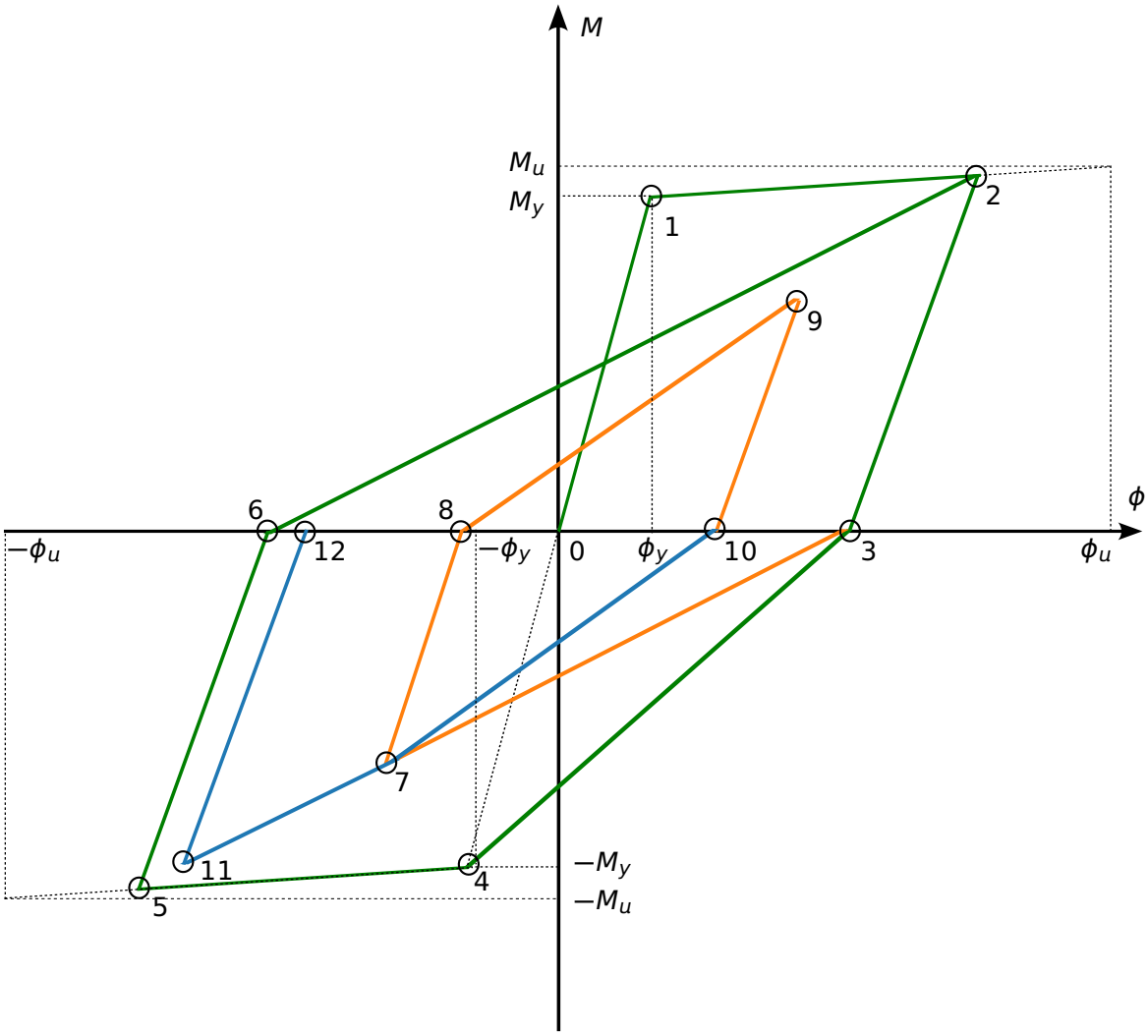


Figure 3: Response of a plastic hinge, following the Modified Takeda hysteretic model for a prescribed cyclic load sequence (cf. Fig. 1)

the elastic stiffness $k_l$, the hardening stiffness $k_h$, and the unloading stiffness $k_u$, respectively:

$$k_l = \frac{M_y}{\phi_y}, \qquad k_h = \frac{M_u}{\phi_u - \phi_y}, \qquad k_u = k_l \left(\frac{\phi_y}{\phi_m}\right)^{\alpha} = k_l \left(\frac{\phi_y}{\phi_2}\right)^{\alpha}, \tag{4}$$

and assume that the reloading factor is $\beta = 0$ for simplicity.

The first loading sequence results in an ”outer” moment-rotation loop with the point sequence ”0–1–2–3–4–5–6–2–3”. The peak positive and negative moments ($M_2$ and $M_5$) in this sequence are larger than the yield moment, meaning they lie on the plastic part of the backbone curve. The unloading branches 2–3 and 5–6 are governed by the unloading stiffness (slope) given in Eq. (4), where $\phi_m = \phi_2 = |\phi_5|$. The loading branch 2–4 progresses towards the negative yield moment, as it has not yet been previously reached, while the slope of the loading branch 6–2 is directed toward $M_2$, which is the largest previously experienced positive moment.

Thus, by applying the rules of the modified Takeda model and simple geometric relationships, the rotation can be obtained analytically for each branch of the first loop:

**Loading 0 – 1:** $M_0 \le M \le M_1\,, \quad \Rightarrow \quad \phi = \dfrac{M}{k_l}\,.$ (5)

**Loading branch 1 – 2:** $M_1 = M_y \le M \le M_u\,, \quad \Rightarrow \quad \phi = \phi_1 + \dfrac{M - M_1}{k_h}\,.$ (6)

**Unloading branch 2 – 3:** $0 \le M \le M_2\,, \quad \Rightarrow \quad \phi = \phi_2 - \dfrac{M_2 - M}{k_u}\,.$ (7)

**Loading branch 3 – 4:** $M_4 = -M_y \le M \le 0\,, \quad \Rightarrow \quad \phi = \phi_3 + \dfrac{M}{\frac{M_4}{\phi_3 - \phi_4}}\,.$ (8)

**Loading branch 4 – 5:** $-M_u \le M \le M_4 = -M_y\,, \quad \Rightarrow \quad \phi = \phi_4 + \dfrac{M - M_4}{k_h}\,.$ (9)

**Unloading branch 5 – 6:** $M_5 \le M \le 0\,, \quad \Rightarrow \quad \phi = \phi_5 - \dfrac{M_5 - M}{k_u}\,.$ (10)

**Loading branch 6 – 2:** $0 \le M \le M_2\,, \quad \Rightarrow \quad \phi = \phi_6 + \dfrac{M}{\frac{M_2}{\phi_2 - \phi_6}}\,.$ (11)

The second loading sequence results in an ”inner” moment-rotation loop with the point sequence ”3–7–8–9–10”. The peak positive and negative moments ($M_7$ and $M_9$) in this sequence are smaller than those in the first, outer loop ($M_2$ and $M_5$); therefore, the slopes of the loading branches 3–7 and 8–9 are dictated by $M_2$ and $M_5$, respectively. The unloading slope $k_u$ of branches 7–8 and 9–10 remains the same, since the maximum deformation from the first, outer loop has not been exceeded.

The rotation of the second loop can thus be obtained analytically for each of its branches:

**Loading branch 3 – 7:** $M_5 \le M \le 0\,, \quad \Rightarrow \quad \phi = \phi_3 - \dfrac{M}{\frac{M_5}{\phi_3 - \phi_5}}\,.$ (12)

**Unloading branch 7 – 8:** $M_7 \le M \le 0\,, \quad \Rightarrow \quad \phi = \phi_7 - \dfrac{M_7 - M}{k_u}\,.$ (13)

**Loading branch 8 – 9:** $0 \le M \le M_2\,, \quad \Rightarrow \quad \phi = \phi_8 + \dfrac{M}{\frac{M_2}{\phi_2 - \phi_8}}\,.$ (14)

**Unloading branch 9 – 10:** $0 \le M \le M_9'\,, \quad \Rightarrow \quad \phi = \phi_9 - \dfrac{M_9 - M}{k_u}\,.$ (15)

Finally, the third loading sequence results in another "inner," but half moment-rotation loop with the point sequence "10–7–11–12". The peak negative moment magnitude $M_{11}$ in this sequence is larger than that of the second loop ($M_7$), but smaller than the peak moment of the first loop ($M_5$). Therefore, when load stepping from point 10 toward point 11, there is a slope change at point 7 (Rule 3 from the previous section). The unloading slope $k_u$ of branches 7–8 and 9–10 remains the same, as the maximum deformation from the first, outer loop has not been exceeded.

The rotation of the third loop can thus be obtained analytically for each of its branches:

$$\textbf{Loading branch 10 – 11:} \begin{cases} M_7 \le M \le 0\,, & \Rightarrow \quad \phi = \phi_{10} - \frac{M}{\frac{M_7}{\phi_{10}-\phi_7}}\,, \\ M_5 \le M \le M_7\,, & \Rightarrow \quad \phi = \phi_7 - \frac{M-M_7}{\frac{M_5-M_7}{\phi_5-\phi_7}}\,. \end{cases} \tag{16}$$

$$\textbf{Unloading branch 11 – 12:} \quad M_{11} \le M \le 0\,, \quad \Rightarrow \quad \phi = \phi_{11} - \frac{M_{11}-M}{k_u}\,. \tag{17}$$

# 3 Numerical Model and Results

The cantilever is modelled with a single beam finite element having a circular cross section with diameter $D$, specific mass $\gamma$, and Young's modulus $E$. Table 2 presents the model properties, plastic hinge properties (backbone moments/rotations and Takeda parameters), and excitation parameters based on the problem description in Sec. 1.

The dynamic time history analysis in SOFiSTiK is carried out using the FEABENCH solver. The standard Newmark-beta algorithm is used for time stepping, with an increment of 0.01 sec and a total time of 1.2 sec, which is sufficient for the complete loading sequence to occur (see Fig. 4). Considering a small loading rate and negligible mass (see Table 2), the system behaves in a quasi-static manner. The convergence criterion for the nonlinear Newton-Raphson solver is set to $1 \times 10^{-7}$.

The analyses are conducted for two values of Takeda's unloading coefficient $\alpha$, assuming the reloading factor $\beta = 0$. Figures 4 and 6 depict the moment-rotation diagrams for unloading coefficients $\alpha = 0.0$ and $\alpha = 0.5$, respectively. Additionally, Table 2 presents results for selected points from Fig. 3. The analytical reference results are obtained using the rules presented previously in Sec. 2 (cf. Eqs. (4)–(17)).

Excellent agreement can be observed between the numerical and analytical curvatures for both unloading factors. Mechanically, it is notable how increasing the unloading factor skews the moment-rotation diagram; thereby, the less strain energy is dissipated.

Table 1: Model Properties

| Model Properties | Hinge Properties | Excitation Properties |
|---|---|---|
| $\gamma = 1 \cdot 10^{-6}\, kN/m^3$ | $M_y = 1000\, kNm$ | $dM/dt = 1000\, kNm/sec$ |
| $E = 1 \cdot 10^{6}\, MPa$ | $M_u = 1400\, kNm$ | $M_2 = -M_5 = 1200\, kNm$ |
| $D = 1\, m$ | $\phi_y = 50\, mrad$ | $M_9 = -M_7 = 800\, kNm$ |
| | $\phi_u = 1000\, mrad$ | $M_{11} = -1000\, kNm$ |
| | $\alpha = 0.0 / 0.5$ | |
| | $\beta = 0.0$ | |

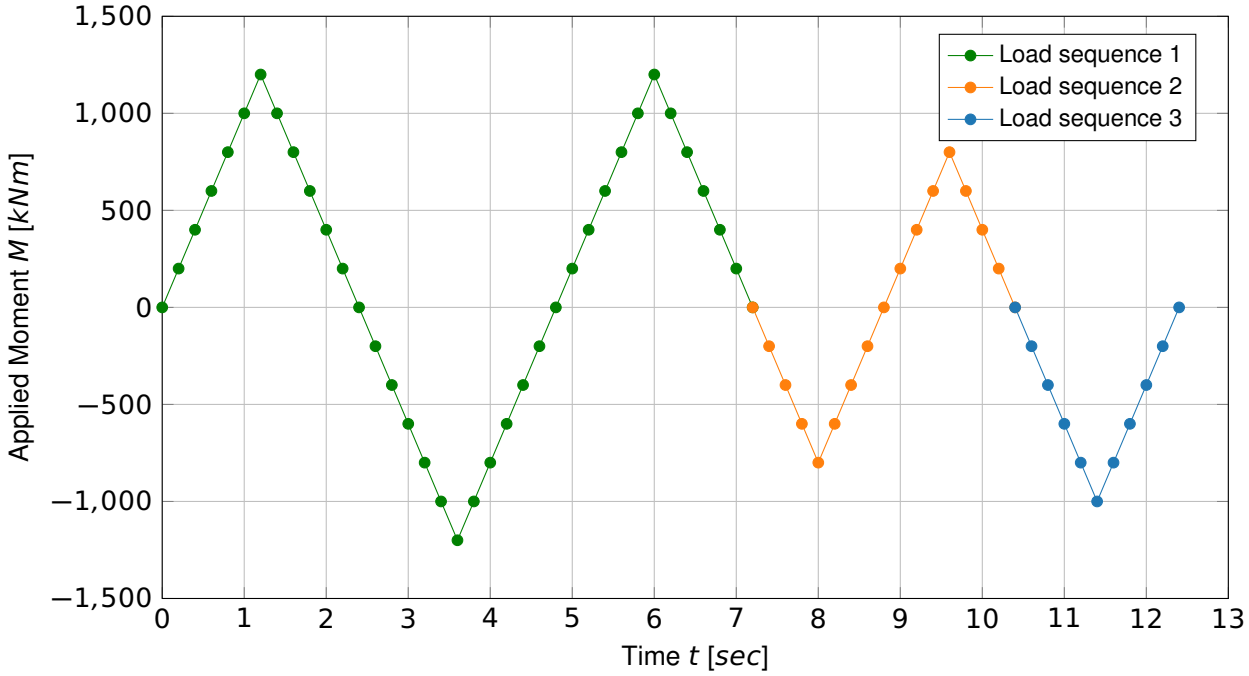


Figure 4: Time history of quasi-static load sequence

Table 2: Analysis results

| | | | $\alpha = 0.0$ | | | $\alpha = 0.5$ | | |
|---|---|---|---|---|---|---|---|---|
| Point | $t$ | $M$ | $\phi_{\text{num}}$ | $\phi_{\text{ref}}$ | $\lvert e_r \rvert$ | $\phi_{\text{num}}$ | $\phi_{\text{ref}}$ | $\lvert e_r \rvert$ |
| [−] | [$sec$] | [$kNm$] | [$mrad$] | [$mrad$] | [%] | [$mrad$] | [$mrad$] | [%] |
| 0 | 0.0 | 0 | 0.00 | 0.00 | 0.00 | 0.00 | 0.00 | 0.00 |
| 1 | 1.0 | 1000 | 50.00 | 50.00 | 0.00 | 50.00 | 50.00 | 0.00 |
| 2 | 1.2 | 1200 | 525.00 | 525.00 | 0.00 | 525.00 | 525.00 | 0.00 |
| 3 | 2.4 | 0 | 465.00 | 465.00 | 0.00 | 330.58 | 330.58 | 0.00 |
| 4 | 3.4 | -1000 | -50.00 | -50.00 | 0.00 | -50.00 | -50.00 | 0.00 |
| 5 | 3.6 | -1200 | -525.00 | -525.00 | 0.00 | -525.00 | -525.00 | 0.00 |
| 6 | 4.8 | 0 | -465.00 | -465.00 | 0.00 | -330.58 | -330.58 | 0.00 |
| 2 | 6.0 | 1200 | 525.00 | 525.00 | 0.00 | 525.00 | 525.00 | 0.00 |
| 3 | 7.2 | 0 | 465.00 | 465.00 | 0.00 | 330.58 | 330.58 | 0.00 |
| 7 | 8.0 | -800 | -195.00 | -195.00 | 0.00 | -239.81 | -239.81 | 0.00 |
| 8 | 8.8 | 0 | -155.00 | -155.00 | 0.00 | -110.19 | -110.19 | 0.00 |
| 9 | 9.6 | 800 | 298.33 | 298.33 | 0.00 | 313.27 | 313.27 | 0.00 |
| 10 | 10.4 | 0 | 258.33 | 258.33 | 0.00 | 183.66 | 183.65 | 0.00 |
| 7 | 11.2 | -800 | -195.00 | -195.00 | 0.00 | -239.81 | -239.81 | 0.00 |
| 11 | 11.4 | -1000 | -360.00 | -360.00 | 0.00 | -382.41 | -382.40 | 0.00 |
| 12 | 12.4 | 0 | -310.00 | -310.00 | 0.00 | -220.39 | -220.39 | 0.00 |

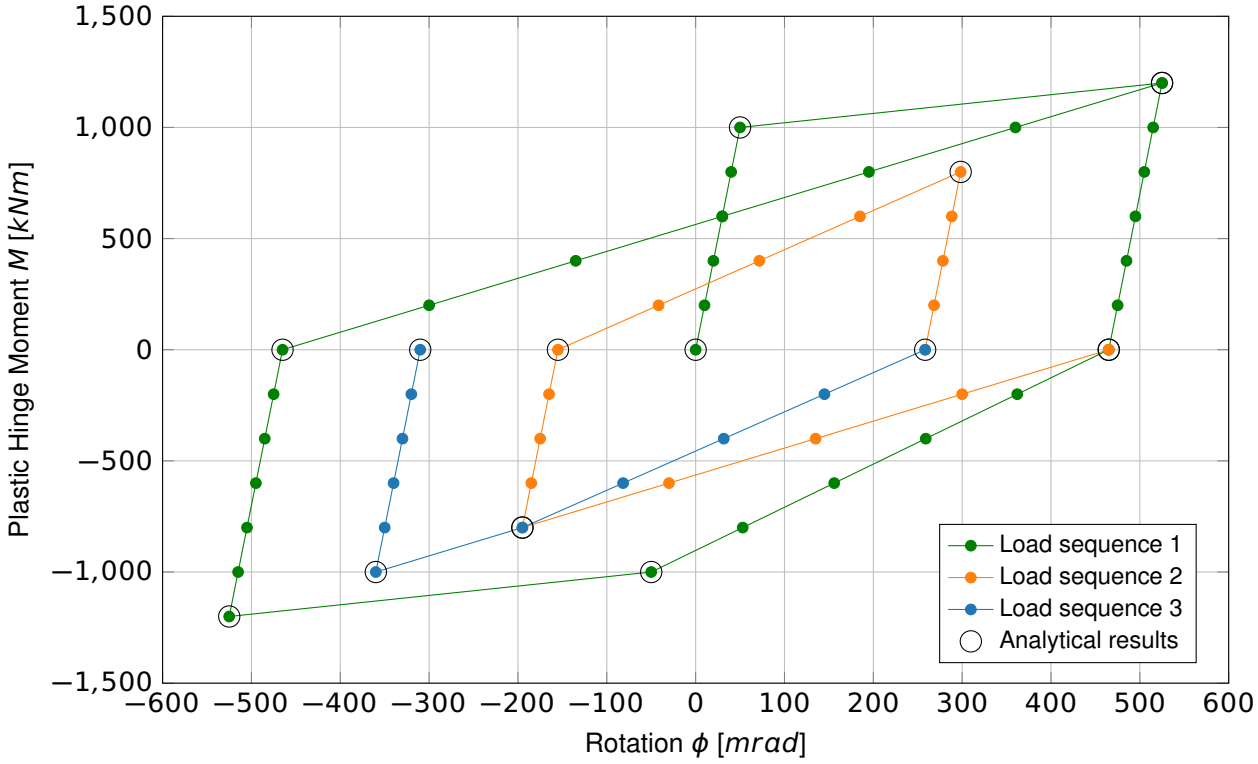


Figure 5: Moment-rotation response of a plastic hinge with Takeda hysteretic model ($\alpha = 0.0$)

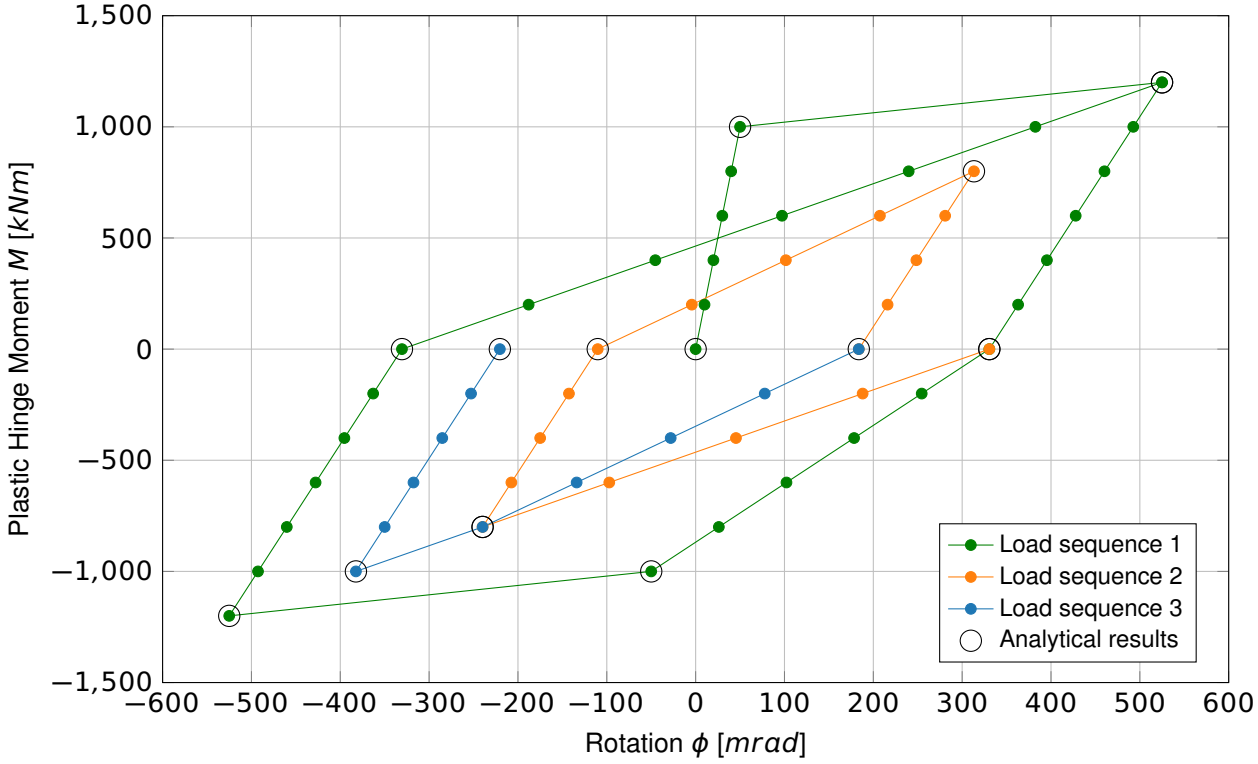


Figure 6: Moment-rotation response of a plastic hinge with Takeda hysteretic model ($\alpha = 0.5$)

# 4 Conclusion

This example investigates the behaviour of an elasto-plastic plastic hinge using the modified Takeda hysteretic model. For a specific cyclic loading protocol, the response of the hinge can be obtained analytically following Takeda's rules for loading and unloading. The results from the nonlinear numerical analysis agree well with the analytical counterparts. This example thus verifies the implementation of the modified Takeda hysteretic model within nonlinear dynamic analysis.

# 5 Literature

[1] N.N. Nielsen T. Takeda M.A. Sozen. "Reinforced concrete response to simulated earthquakes". In: *Journal of the Structural Division, Proceedings of the American Society of Civil Engineers* (1970).
[2] A. J. Carr. "RUAUMOKO-3D - A program for inelastic time-history analysis". In: (2004).